Atomic cranks and levers control sugar ring conformations

2005 J. Phys.: Condens. Matter 17 S1427

(http://iopscience.iop.org/0953-8984/17/18/001)

INSTITUTE OF PHYSICS PUBLISHING JOURNAL OF PHYSICS: CONDENSED MATTER

J. Phys.: Condens. Matter **17** (2005) S1427–S1442 doi:10.1088/0953-8984/17/18/001

Atomic cranks and levers control sugar ring conformations

Qingmin Zhang, Gwangrog Lee and Piotr E Marszalek

Center for Biologically Inspired Materials and Material Systems, Department of Mechanical Engineering and Materials Science, Duke University, Durham, NC 27708, USA

E-mail: pemar@duke.edu

Received 30 November 2004, in final form 4 January 2005
Published 22 April 2005
Online at stacks.iop.org/JPhysCM/17/S1427

Abstract

In this paper we review the conformational analysis of sugar rings placed under tension during mechanical manipulations of single polysaccharide molecules with the atomic force microscope and during steered molecular dynamics simulations. We examine the role of various chemical bonds and linkages between sugar rings in inhibiting or promoting their conformational transitions by means of external forces. Small differences in the orientation of one chemical bond on the sugar ring can produce significantly different mechanical properties at the polymer level as exemplified by two polysaccharides: cellulose, composed of β-1 $\rightarrow$ 4-linked D-glucose, and amylose, composed of α-1 $\rightarrow$ 4-linked D-glucose. In contrast to β-glucose rings, which are mechanically stable and produce simple entropic elasticity of the chain, α-glucose rings flip under tension from their chair to a boat-like structure and these transitions produce deviations of amylose elasticity from the freely jointed chain model. We also examine the deformation of two mechanically complementary 1 $\rightarrow$ 6-linked polysaccharides: pustulan, a β-1 $\rightarrow$ 6-linked glucan, and dextran, a α-1 $\rightarrow$ 6-linked glucan. Forced rotations about the C_5–C_6 bonds govern the elasticity of pustulan, and complex conformational transitions that involve simultaneous C_5–C_6 rotations and chair–boat transitions govern the elasticity of dextran. Finally, we discuss the likelihood of various conformational transitions in sugar rings in biological settings and speculate on their significance.

(Some figures in this article are in colour only in the electronic version)

1. Introduction

Polysaccharides are polymers of sugar monomers, such as glucose, which is composed of carbon and oxygen atoms connected into a ring-like structure with side groups made of oxygens and hydrogens (Rao *et al* 1998). Carbon atoms of neighbouring rings are connected by oxygen

atoms by the so-called glycosidic linkage to form very long polysaccharide chains (∼10–10 000 units) whose common names depend on the unit sugar and the type of connection between the sugar rings (Rao *et al* 1998). For example, when the sugar unit is β-D-glucose (figure 2(B), inset) and the glycosidic linkage connects carbon atom No 1 on one ring to carbon atom No 4′ on the next ring, the polysaccharide formed is ubiquitous cellulose. However, when $1 \rightarrow 4$ linkages connect α-D-glucose units, the polysaccharide formed is amylose (figure 3(A), inset), a component of starch. The only difference between β- and α-D-glucose is in the orientation of the C_1–O_1 bond relative to the plane of the ring structure. In β-D-glucose, this bond is *equatorial* (in the plane of the ring; figure 2(B), inset), but in α-D-glucose this bond is *axial*, (perpendicular to the ring; figure 3(A), inset). Considering the very small chemical difference between cellulose and amylose, a question is in order: why does cellulose play a fundamental structural role for all land plants, while amylose does not play any structural role but is commonly used to store energy in many plants (e.g. corn and potato are full of starches)? Clearly, the anomeric configuration of the glycosidic bond of β-D-glucose promotes the type of crystallization that allows the formation of cellulose fibres. However, we hypothesize that β-linkages have an additional role in that they *mechanically* stabilize the chair conformation of the sugar ring under tensile forces, while α-linkages, under similar forces would induce undesired conformational instability of the glucose ring. These different elastic properties of the glucose ring rendered by α- and β-linkages were investigated in recent stretching experiments on single cellulose and amylose chains that were carried out with the atomic force microscope (AFM) (Rief *et al* 1997, 1998, Marszalek *et al* 1998, 1999a, 1999b, 2001, 2002, Li *et al* 1998, 1999, Brant 1999, Lee *et al* 2004a, 2004b). These studies point to the linkage-dependent configurational flexibility of the sugar rings as an important determinant of polysaccharide elasticity. Although the flexibility of monomeric sugar rings was investigated in the past (Pensak and French 1980, French *et al* 1990), the elastic properties of polysaccharides have rarely been addressed by computer modelling. We present here some recent results of steered molecular dynamics simulations of polysaccharide elasticity, which provide an insight into conformational events triggered in sugar rings by applied forces and point to the origin of the difference between the elasticity of cellulose and amylose. In the second part of this paper, we present interesting mechanical properties of two $1 \rightarrow 6$-linked polysaccharides: pustulan and dextran (Rief *et al* 1997, Marszalek *et al* 1998). Their elasticity is governed by atomic cranks that rotate chemical groups and atomic levers that flip the sugar ring into a boat-like conformation (Lee *et al* 2004a, 2004b). These studies, by examining the relationship between sugar chemistry and mechanics, have expanded the conformational analysis of ring structures (Barton 1970) to include force-induced structural changes as so far unrecognized mechanochemical events that may have significance in biological systems (Marszalek *et al* 1998, 1999a, 1999b, Lee *et al* 2004a, 2004b).

2. Single-molecule force spectroscopy (SMFS)

Force spectroscopy examines the relationship between a molecule's length and tension (Rief *et al* 1997). Mechanical manipulations of single molecules with atomic force microscopy (AFM) and optical tweezers revealed, through force spectroscopy measurements, a wealth of interesting details about biopolymer elasticity (Fisher *et al* 2000, Bustamante *et al* 2000, 2003). It appears that biopolymers such as DNA, proteins and most polysaccharides behave as freely jointed chains (FJC) (Flory 1953) or worm-like chains (WLC) (Bustamante *et al* 1994) with a simple entropic elasticity, only for a limited range of forces/extensions. At higher forces they typically undergo a range of structural rearrangements, that reveal themselves as

distinct deviations from the FJC/WLC models of entropic elasticity (Marszalek *et al* 1999b, 2003, Fisher *et al* 2000, Bustamante *et al* 2003).

3. Materials and methods

3.1. Polysaccharides

The experiments described in this paper were carried out on several commercially available polysaccharides: methylcellulose (M-0512; degree of substitution DS = 0.4; Sigma); amylose (A-0512, type III: from potato; Sigma); pectin (P-9135, from citrus fruits; Sigma); pustulan, from the lichen *Umbilicaria pustulata* (#400 507, lot# 5-662R3, Carbomer, Inc., San Diego, CA); dextran (T500, T2000, Pharmacia/Pfizer, Peapack, NJ). Methylcellulose, pectin, pustulan and dextran were dissolved in water at a concentration of 0.001–5% (w/v). Amylose was solubilized by wetting with ethanol (100 mg ml^{-1}), followed by treatment with sodium hydroxide (10%) and heating. A layer of polysaccharide molecules was created by drying a drop of these solutions on glass cover-slips. Then the dehydrated sample was rinsed extensively with water to leave only those molecules that are tightly attached to the glass surface (Li *et al* 1998). After drying the sample and placing it in the AFM, the fluid cell was filled with an appropriate solvent for force spectroscopy measurements. The measurements were carried out in water (methylcellulose, amylose, pustulan and dextran) or in PBS buffer (pectin). In order to pick polysaccharide molecules for stretching measurements, an AFM tip was pressed down onto the sample for 1–3 s and at forces of 10–40 nN and then retracted.

3.2. AFM instruments

Force spectroscopy measurements were carried out on two AFM instruments: the PicoForce from Veeco Metrology Group, (Santa Barbara, CA) and a home-built AFM, which was equipped with a piezoelectric actuator with a strain gauge sensor from Physik Instrumente, and the so-called low noise AFM head designed for the MultiMode AFM, from Veeco. This latter AFM is similar to that described in (Oberhauser *et al* 1998). The spring constant of each AFM cantilever (Si_3N_4, Veeco, Santa Barbara, CA) was calibrated in solution, using the thermal noise method described in (Florin *et al* 1995).

3.3. Interpretation of SMFS results

Figure 1 illustrates the principles of single-molecule force spectroscopy as implemented on the AFM platform. The figure shows examples of force–extension curves obtained by force spectroscopy on methylcellulose (MC) in water and illustrates the molecular arrangements between the substrate and the AFM tip that produce such force–extension relationships (force spectrograms). In contrast to native cellulose, which is very difficult to dissolve, the methyl derivative of cellulose can be easily dissolved in water and is a good polysaccharide model for force spectroscopy measurements in the AFM. The trace shown in figure 1(A) represents a force–extension curve obtained on several MC molecules that adsorbed to the AFM tip, and were stretched simultaneously (in parallel). This situation is illustrated in figure 1(B). Since the molecular fragments are picked up by the AFM tip randomly, they are of different lengths. Upon the movement of the substrate away from the tip, the shortest fragment is stretched first, while the other two molecules are still relaxed and generate little force (figure 1(B)). With the substrate movement continuing, the other two molecules would be stretched and detached successively. This situation creates a mechanically complex system, which produces a complicated, very difficult to interpret, force spectrogram with several

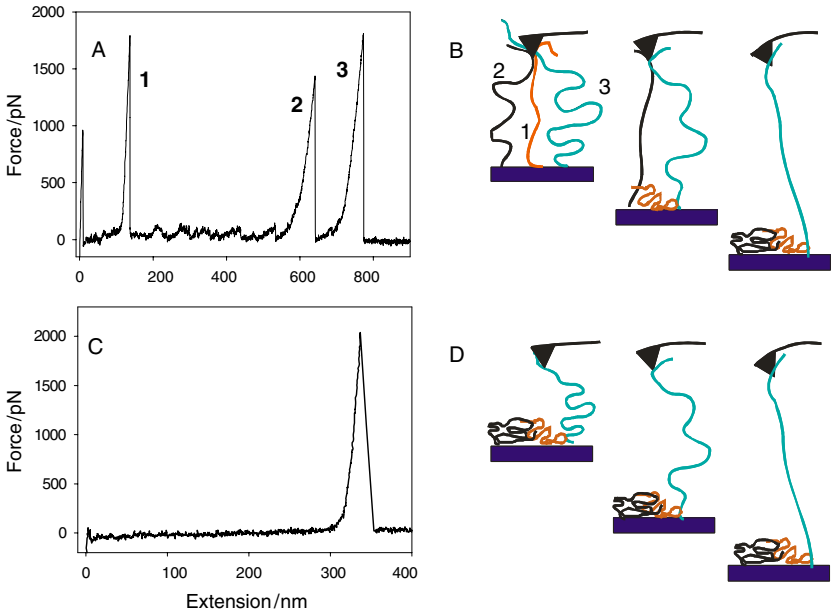

Figure 1. AFM measured force spectrograms of methylcellulose in water. (A) A force spectrogram representing a simultaneous stretching of several molecules of different lengths. (B) A schematic diagram illustrating the molecular configuration which generated the force spectrogram shown in (A). (C) A single-methylcellulose-molecule force spectrogram. (D) A single-molecule configuration for force spectroscopy measurements.

partially overlapping force peaks (figure 1(A)). However, when there is only one molecule between the tip and the substrate, the force spectrogram is characterized by a flat baseline, followed by a single force peak (figures 1(C) and (D)). Such spectrograms are characteristic of single molecules and they overlap well after the normalization of the molecule extension.

3.4. Extension normalization procedures

Figure 2 shows several force–extension curves of single MC fragments obtained in *separate* experiments and plotted on a common graph. The contour lengths of the MC fragments are different and they vary over a wide range (figure 2(A)). To compare these recordings we need to normalize the molecule extension. The freely jointed chain model states that the chain extension, x, at any given force, F, is proportional to the contour length of the polymer, L_c:

$$x(F) = L_c\left\{\coth\left(\frac{l_K F}{k_B T}\right) - \frac{k_B T}{l_K F}\right\}$$

where l_K is the length of the Kuhn segment, k_B is the Boltzmann constant and T is the absolute temperature (Flory 1953). Thus, when we divide the FJC's extension, x, by the extension $x(F_0)$ determined at a certain force, F_0, we obtain the relationship between extension and force, independent of the chain contour length, L_c. The extension at other forces then becomes a percentage of the extension generated by F_0, which becomes (the extension) 1 after this normalization. By choosing F_0 common to all recordings, e.g. the highest common force achieved for a set of force spectrograms, and normalizing each recording, we can compare the family of such recordings. Typically, the normalized recordings for the same type of polymer overlap, regardless of their contour lengths (figures 2(B), 3(A)).

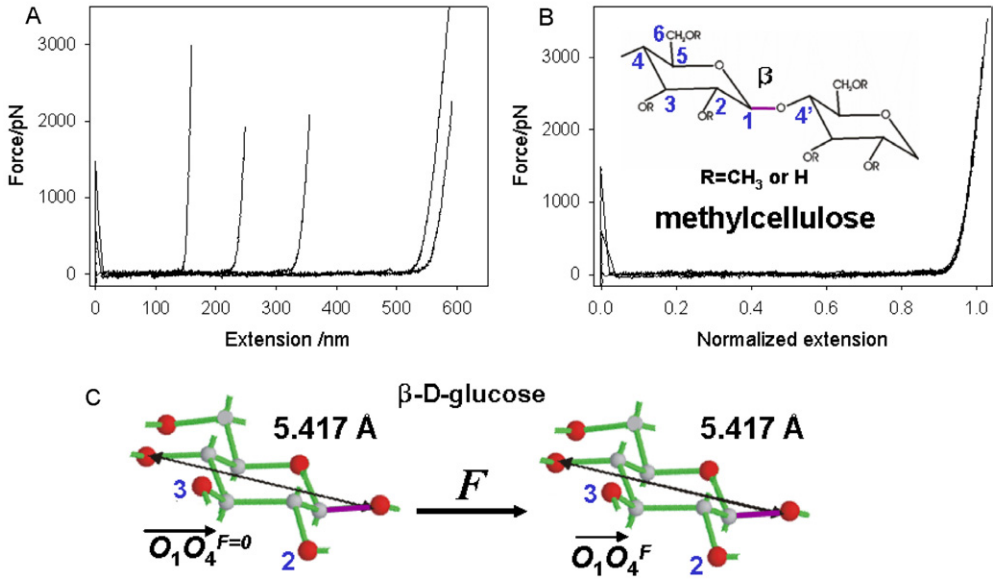

Figure 2. (A) Force spectrograms of single methylcellulose molecules of various lengths. (B) Normalized force spectrograms of five curves from (A). Inset: the structure of methylcellulose showing two β-D-glucopyranose rings connected by $1 \rightarrow 4$ linkage. (C) The *ab initio* optimized chair structure of β-D-glucose. This ground energy structure provides the maximum separation of the glycosidic oxygen atoms O_1–O_4, and minimum torque on the ring when a stretching force is applied to the C1–O1 bond. Therefore this structure is stable during stretching.

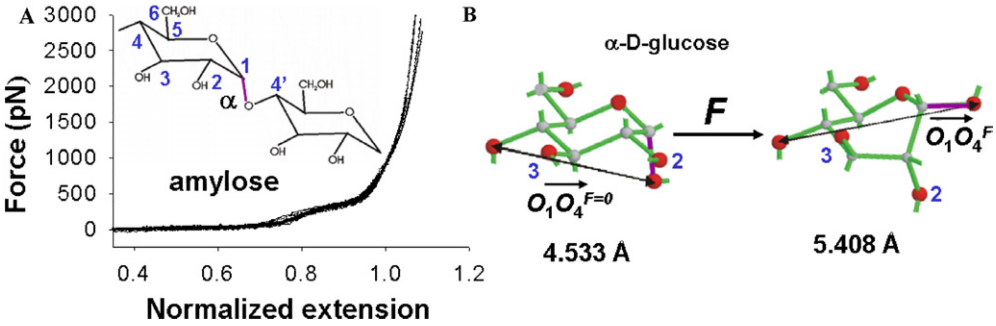

Figure 3. (A) Typical force–extension curves of amylose. Inset: the structure of amylose showing two α-D-glucopyranose residues connected by $1 \rightarrow 4$ linkage. (B) *Ab initio* optimized structures of α-D-glucose in the chair and boat conformations. The separation of the glycosidic oxygen atoms, O_1–O_4, increases during stretching upon the chair–boat transition.

4. Cellulose elasticity: a freely jointed chain composed of rigid rings

In figure 2(B) we show the normalized force spectrograms measured by AFM on single molecules of methylcellulose (Li *et al* 1998, 1999, Marszalek *et al* 1999a, 1999b, 2001). These recordings overlap, supporting our assumption that they were obtained for single molecules. Moreover, these recordings are indicative of simple entropic elasticity that can be described by the FJC model, suggesting that single cellulosic chains behave as simple entropic springs. Figure 2(C) shows the result of the *ab initio* geometry optimization of β-D-glucose and of

calculations of the separation of glycosidic oxygen atoms, O_1–O_4. The results indicate that cellulose monomers have the maximum O_1–O_4 length in the ground energy chair conformation, and that this separation would decrease in other conformations higher in energy, such as boat-like structures (not shown). Therefore, cellulose monomers do not undergo conformational transitions during stretching, but only experience slight deformations (elongation).

5. Amylose elasticity: chair–boat transitions of sugar rings

5.1. Force spectrograms of amylose obtained by AFM

In contrast to that of cellulose, amylose elasticity shows a large deviation from the FJC model, which is evident as a characteristic plateau feature that occurs at a force of 275 ± 45 pN (figure 3(A)) (Marszalek *et al* 1998, Li *et al* 1999). Clearly the axial (perpendicular) orientation of the C_1–O_1 bonds in amylose must be somehow responsible for amylose elasticity deviating from that of a simple entropic (cellulosic) chain. The examination of forces acting on the glucose ring during the stretch indicates that in the case of α-D-glucose (amylose), the force attached at the glycosidic oxygen atom O_1 produces a significant torque on the ring structure, with the C_1–O_1 bond acting as the lever arm, and the C_2–O_5 (ring) line acting as an imaginary axis of rotation. This torque flips the ring structure from its ground energy 'chair' conformation to a 'boat-like' conformation higher in energy. As shown by the *ab initio* quantum mechanical geometry optimization, this boat conformation increases the separation of the O_1 and O_4 atoms by $\sim$0.9 Å, about 19% of the initial length (figure 3(B)) (Marszalek *et al* 1998). On the basis of this simple mechanistic model supported by quantum mechanical calculations, we proposed that the plateau feature in amylose elasticity represents a concerted transition of the glucose rings from their short chair structures to their extended, boat-like configuration (Marszalek *et al* 1998).

5.2. Steered molecular dynamics simulation of amylose elasticity

To gain additional insight into the behaviour of glucose rings in amylose subjected to tensile forces and to verify our conjecture about force-induced chair–boat transitions, we carried out molecular dynamics simulations of the stretching process. We used the so-called steered molecular dynamics protocol (SMD) (Izrailev *et al* 1997, Isralewitz *et al* 2001, Gao *et al* 2002, Grubmüller *et al* 1996). In this approach one terminal atom of the amylose chain composed of ten rings is constrained and the other terminal atom is subjected to a harmonic potential, whose centre is moving at a constant speed in the stretching direction, simulating the AFM measurement. The results of our SMD calculations of amylose, using the program NAMD (Kalé *et al* 1999) and X-PLOR (Brunger 1992) and a new force field developed for carbohydrates (Kuttel *et al* 2002) and an implicit solvent model, are shown in figure 4(A), which also compares the simulation with the AFM data. We see that the calculation produces a plateau feature in the force–extension profile, which is similar to the plateau captured by the AFM. The analysis of the trajectories of the ten rings of the amylose chain modelled by the SMD simulation (cf an example of such an analysis for ring No 6, figure 4(B)), indicates that 40–50% of the rings undergo a transition to a boat-like structure during the plateau phase of the stretch. These transitions account for the most of the amylose lengthening in the plateau region, with some length contribution ($\sim$25%) generated also by rotations around the glycosidic linkages. The rest of the rings flip to a boat-like conformation at somewhat greater extensions immediately following the plateau feature. Our SMD result obtained with the use of an implicit water model is similar to the result obtained on amylose using the quantum mechanics-based

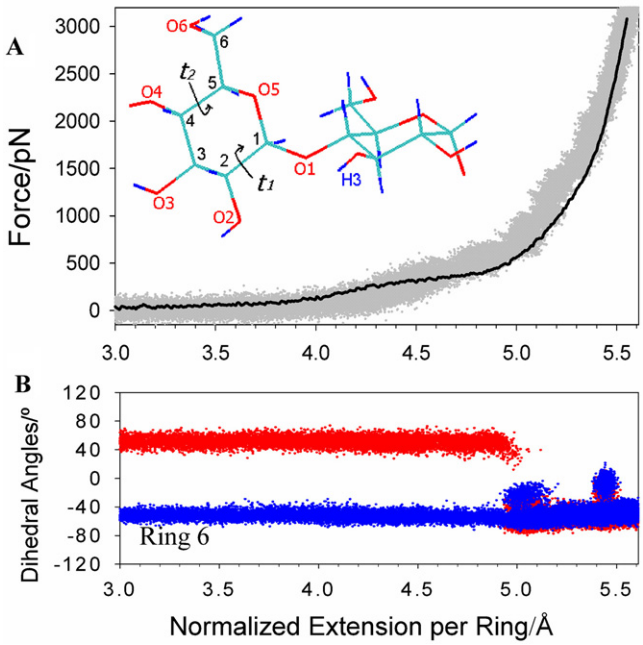

Figure 4. A 1 μs SMD simulation of amylose reproduces the AFM stretching curve. (A) A comparison between normalized force–extension curves of amylose obtained by AFM (black trace) and by SMD simulation (grey trace). Inset: the structure of amylose showing the numbering of carbon and oxygen atoms and torsions, t_1 and t_2. (B) The conformational dynamics of ring No 6 during the 1 μs simulation as revealed by the two torsions: $t_1 = O_1$–C_1–C_2–O_2 (dark grey trace) and $t_2 = O_5$–C_5–C_4–C_3 (black trace) which indicate the conformational status of the glucose ring.

SMD method and explicit water, where 50%–60% of the rings changed their conformation during the plateau phase (Lu *et al* 2004). Thus, our simulations support our model of amylose elasticity as being governed by force-induced conformational transitions of α-D-glucose rings.

6. Comparison of the elasticity of cellulose and amylose

It is interesting that polymers, whose chemical structures differ only by the orientation of one bond (C_1–O_1) and are otherwise identical, display such different mechanical properties. We pointed out that the perpendicular orientation of this bond relative to the plane of the glucose ring in amylose creates a conformational instability during stretching. In the case of cellulose (β-D-glucose) this bond is equatorial (almost parallel to the ring) and the stretching force produces minimal torque on the sugar ring. Therefore, the stretching forces do not trigger any major structural change in the glucose rings, but merely cause their slight deformation (Marszalek *et al* 1999a, 1999b, Li *et al* 1999, O'Donoghue and Luthey-Schulten 2000). In addition, in β-D-glucose, the separation of the O_1 and O_4 atoms in boat-like structures, is, unlike in amylose, actually shorter than in the ground energy chair conformation. Therefore, under stretching conditions, chair–boat transitions are prohibited in cellulose. We hypothesize that the increased conformational stability of the glucose rings rendered by β-1 $\rightarrow$ 4 linkages as compared to α-1 $\rightarrow$ 4 linkages contributes to the strength of cellulose-built structures. Single molecules of cellulose are arranged in extremely strong and rigid microfibrils, which are the building block of the cell wall in plant cells. In the fibril, cellulosic chains interact among themselves through a network of hydrogen bonds (Jarvis 2003, Nishiyama *et al* 2003).

If the glucose rings in cellulose were, as in amylose, prone to conformational instabilities, the precise network of hydrogen bonds would be destroyed under tension and the fibril would be severely weakened. This situation is illustrated in figures 2(C) and 3(B). The OH groups marked as 2 and 3, which in cellulose participate in the intermolecular hydrogen bonding with the rings from another chain, do not change their orientation under tension (figure 2(C)), because the ring stays all the time in the chair conformation. However, in amylose, these two groups reorient themselves from the equatorial position in the chair conformation, to the perpendicular orientation in a boat-like structure (figure 3(B)). Thus, we postulate that β-1 $\rightarrow$ 4 linkages not only promote the type of crystallization needed to form cellulose fibres, but they also mechanically stabilize the conformation of the sugar rings required in strong fibres.

7. The molecular elasticity of pectin

The role of axial glycosidic linkages in the elasticity of polysaccharides was investigated further by means of force spectroscopy measurements on single molecules of pectin (Marszalek *et al* 1999a). Pectin is a polymer composed of α-D-galactopyranuronic acid sugar units linked by 1 $\rightarrow$ 4 linkages (figure 5(A), inset). The basic structure of the galactopyranuronic acid sugar ring of pectin is the same as that of α-D-glucose. However, while in glucose the C_4–O_4 bond is equatorial, in galactose this bond is oriented axially. The other difference between glucose and galactopyranuronic acid is that there is an acid group attached to carbon atom C_6. Since this group is not part of the linkage, its mechanical role is rather insignificant. Thus, the most important structural feature of pectin is the axial orientation of both bonds of the glycosidic linkage, i.e. C_1–O_1 and O_1–C_4. In contrast to cellulose, where the stretching forces produce minimal torque on the ring, and amylose, where only the force attached to the C_1–O_1 bond produces significant torque, we expect that in pectin both bonds, C_1–O_1 and O_1–C_4, will provide lever arms and will produce a pair of forces with significant torque on the ring. Figure 5(A) shows normalized force spectrograms of pectin in water obtained by AFM. These spectrograms reveal two distinct plateau features: one similar to that for amylose occurs at around 300 pN and the second plateau starts at $\sim$800 pN. It seems that the C_1–O_1 and O_1–C_4 bonds work as a pair of atomic levers, which flip the pectin ring from a chair to a boat-like conformation, and this transition produces the first plateau. Then, they flip the boat-like structure to an inverted chair conformation (Pickett and Strauss 1970) and that transition produces the second plateau. This interpretation of pectin force spectrograms is supported by the *ab initio* geometry optimization of the pectin ring in various conformations, which indicates that the O_1–O_4 distance increases during both transitions by amounts which are consistent with the AFM data (figure 5(B)).

We summarize by observing that there seems to be a clear link between the number of axial bonds (per monomer) in 1 $\rightarrow$ 4-linked polysaccharides and the number of plateaus in their force spectrograms. Cellulose has all its bonds in the equatorial deposition and follows the FJC model with no plateau, amylose has one axial bond (at C_1) and reveals one plateau and pectin has two axial bonds and two plateaus (Marszalek *et al* 1999a). We also note that the final conformation of the sugar rings stretched by external forces has in each case the glycosidic linkages oriented equatorially, which minimizes torque on the ring and provides the maximum separation between the glycosidic oxygen atoms.

8. Dextran and pustulan: elasticity controlled by 1 $\rightarrow$ 6 linkages

In contrast to cellulose, amylose and pectin, which all exploit 1 $\rightarrow$ 4 linkages, dextran and pustulan are two examples of glucose-based polysaccharides that exploit uncommon 1 $\rightarrow$ 6

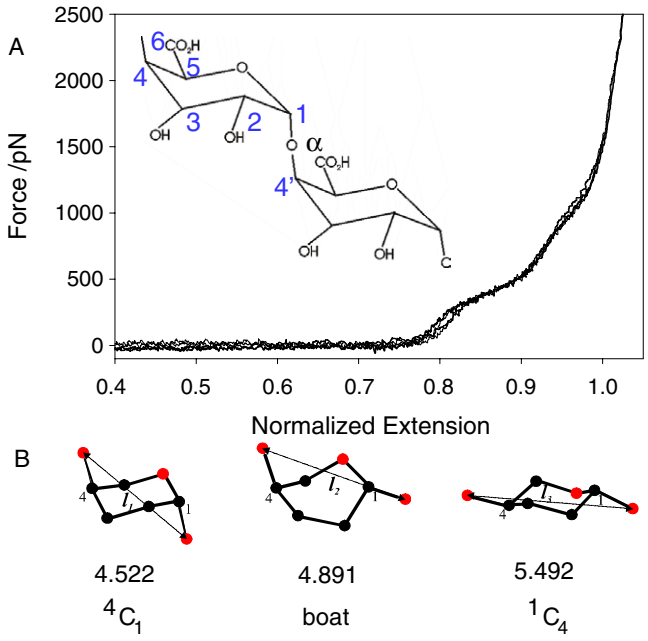

Figure 5. (A) Normalized force–extension curves of pectin. Inset: the structure of pectin showing two α-D-galactopyranuronic acid rings connected by $1 \rightarrow 4$ linkage. (B) *Ab initio* calculations of the separation of glycosidic oxygen atoms during chair inversion of the pectin monomer.

linkages, where carbon atom C_1 on one glucose ring is connected by a glycosidic oxygen atom to carbon atom C_6 on the next ring. These linkages deserve special attention for two reasons. First, in contrast to $1 \rightarrow 4$ linkages, which transmit the stretching forces to the pyranose ring along its axis of symmetry, $1 \rightarrow 6$ linkages attach the force vector to the sides of the ring. Second, they include an additional bond in the linkage, C_5–C_6 (figures 6, 7, 8, inset), about which restricted rotations occur, increasing the mechanical complexity of $1 \rightarrow 6$-linked sugars. Therefore, such linkages can generate complex deformations of the pyranose ring, which defy simple analysis. Interestingly, pustulan and dextran are, like cellulose and amylose, mechanically complementary. Pustulan is composed of β-D-$1 \rightarrow 6$-linked glucose units (Lindberg and McPherson 1954, Hellerqvist *et al* 1968) and dextran is composed of α-D-$1 \rightarrow 6$-linked glucose units (Whistler and BeMiller 1993). We begin with the description of the elasticity of pustulan, which was measured recently by Lee *et al* (2004a, 2004b).

8.1. Pustulan elasticity: AFM measurements

Pustulan, like cellulose, has β-linkages, but its elasticity (figure 6, middle trace) clearly deviates from that of methylcellulose (figure 6, black dashed trace). This deviation is particularly pronounced in the force regions of 100 and 700 pN, where pustulan elasticity displays almost a Hookean relationship between force and length—a property typical of springs, not polymers. This observation indicates that the mechanical properties of β-$1 \rightarrow 6$ linkages are significantly different from the β-$1 \rightarrow 4$ linkages of methylcellulose. In methylcellulose these linkages behave as if they belonged to a freely jointed chain. Thus they must not experience any rotational restrictions. It seems that the bonds in pustulan do experience rotational restrictions, and higher forces, as compared to those in methylcellulose, are needed to fully extend the

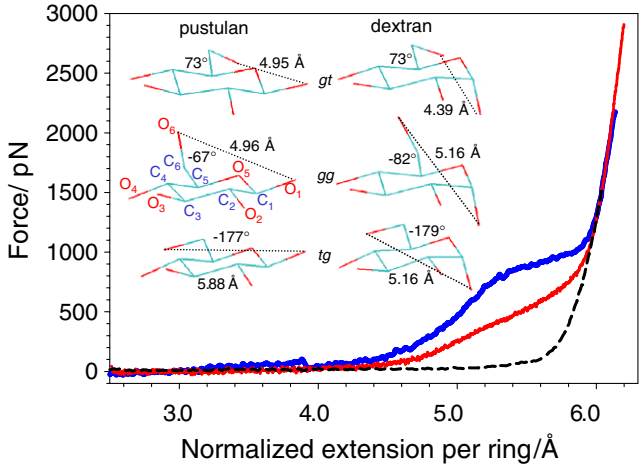

Figure 6. A comparison of normalized force–extension curves of pustulan (middle trace), dextran (top trace) and methylcellulose (black dashed trace). Inset: *ab initio* optimized rotamers (gt, gg, tg) of 1 → 6-linked β-D- and α-D-glucose. The O_6–O_1 distance is shown together with ω torsion for all rotamers. The second ring in the left panel shows the numbering of carbon and oxygen atoms in the glucose ring used to define torsions ω, t_1 and t_2 (see the text). (Adapted from Lee *et al* (2004b).)

pustulan chain (see figure 6). It seems that the rotation of the O_6–C_6 bond about the C_6–C_5 bond is restricted, because this rotation occurs in pustulan but is absent in methylcellulose. This rotation can be characterized by the torsional (dihedral) angle $\omega = O_6$–C_6–C_5–O_5 (figure 6, inset). Three stable orientations are possible for the C_6–O_6 bond, which correspond to $\omega = 60°$ (gt); $\omega = -60°$ (gg) and $\omega = 180°$ (tg) (figure 6, inset). Structural measurements (x-ray and NMR) and numerous calculations show a preference of the glucose monomer towards gt and gg rotameric orientations, which are populated almost equally, with a nearly complete absence of the tg rotamer (gg/gt/tg/ 60:40:0) (Weimar *et al* 1999, Barrows *et al* 1995, Momany and Willett 2000, Kirschner and Woods 2001, Tvaroška *et al* 2002, Appell *et al* 2004). The *ab initio* geometry optimization of the gt, gg and tg rotamers shows that the distance between the glycosidic oxygen atoms is O_1–$O_6 = 5.88$ Å in the tg conformation, and this is about 19% greater than in the gt and gg conformations (O_1–$O_6 = 4.95$ and 4.96 Å, respectively). The length increase of the pustulan chain between 100 and 800 pN measured by AFM is ∼23% (figure 6, middle trace) suggesting that the Hookean elasticity of pustulan is governed by forced gt → tg and gg → tg rotations. Thus, the O_6–C_6 bonds in pustulan seem to work as 'atomic cranks' that swing and rotate between different positions when acted upon by external forces (Lee *et al* 2004a, 2004b).

8.2. SMD simulations of pustulan: forced rotations about C_5–C_6 bonds

Figure 7(A) compares the results of the AFM stretching measurements of pustulan to the result of a 1 μs SMD simulation performed on a pustulan fragment composed of ten glucose rings in an implicit water solvent (Lee *et al* 2004a, 2004b). The agreement between the experiment and the calculation is very satisfactory. The conformational behaviour of the glucose rings and the C_6–O_6 bonds during the 1 μs simulation was followed by monitoring three dihedral angles: $\omega = O_6$–C_6–C_5–O_5 indicates the rotameric status about the C_6–C_5 bond, while $t_1 = O_1$–C_1–

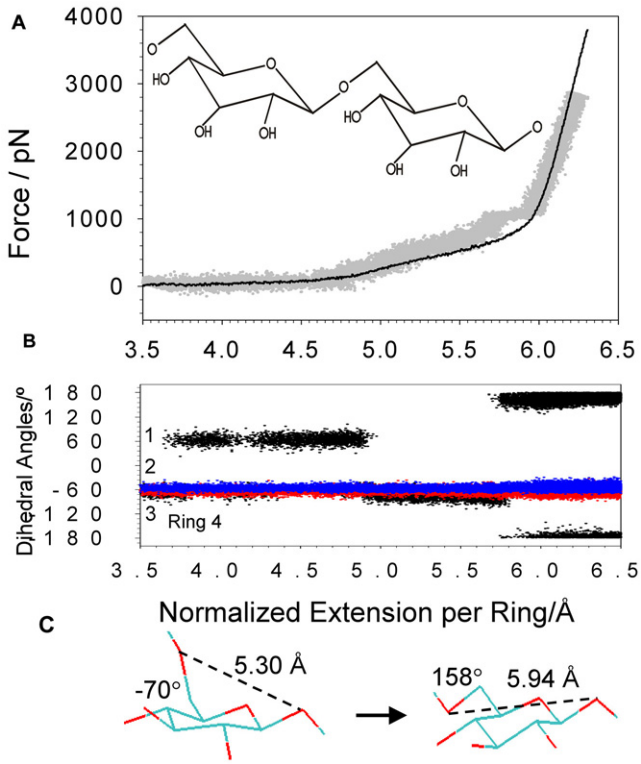

Figure 7. A 1 μs SMD simulation of pustulan reproduces the AFM stretching curve. (A) A comparison between normalized force–extension curves of pustulan obtained by AFM (black trace) and by SMD (grey trace). Inset: the structure of pustulan showing two β-D-glucopyranose rings connected by 1 $\rightarrow$ 6 linkage. (B) The conformational dynamics of ring No 4 during a 1 μs simulation as revealed by the three torsions: $\omega = O_6$–C_6–C_5–O_5 (trace 1), $t_1 = O_1$–C_1–C_2–O_2 (trace 3) and $t_2 = O_5$–C_5–C_4–C_3 (trace 2). (C) Two structures of ring No 4, immediately before and after the gg $\rightarrow$ tg transition.

C_2–O_2 and $t_2 = O_5$–C_5–C_4–C_3 (figure 6, inset) indicate chair–boat transitions. In figure 7(B), we plot the values of these torsions as a function of the normalized extension of the chain for ring No 4, which started in the gg state and whose behaviour is typical of all rings. First, we note that the torsions t_1 and t_2 remained constant for all the rings indicating no chair–boat transitions. Second, all the rings ended the stretching process as tg rotamers, which provide the greatest separation for the glycosidic oxygens O_1 and O_6. From the analysis of the SMD calculation, it can be concluded that the Hookean elasticity of pustulan is governed by forced rotations of the O_6–C_6 'crank' about the C_5–C_6 bond, which shift the distribution of the rotamers from the less energetic and shorter gt and gg conformers to the more energetic and longer tg rotamers (Lee *et al* 2004a, 2004b). It is important to emphasize that, in agreement with our expectations about the equatorial bonds inhibiting chair–boat transitions, all the rings in pustulan preserve their chair conformation during the stretching process.

8.3. Dextran elasticity: AFM measurements

Dextran was the first polysaccharide on which measurements by single-molecule force spectroscopy were made using the AFM instrument (Rief *et al* 1997). Dextran elasticity,

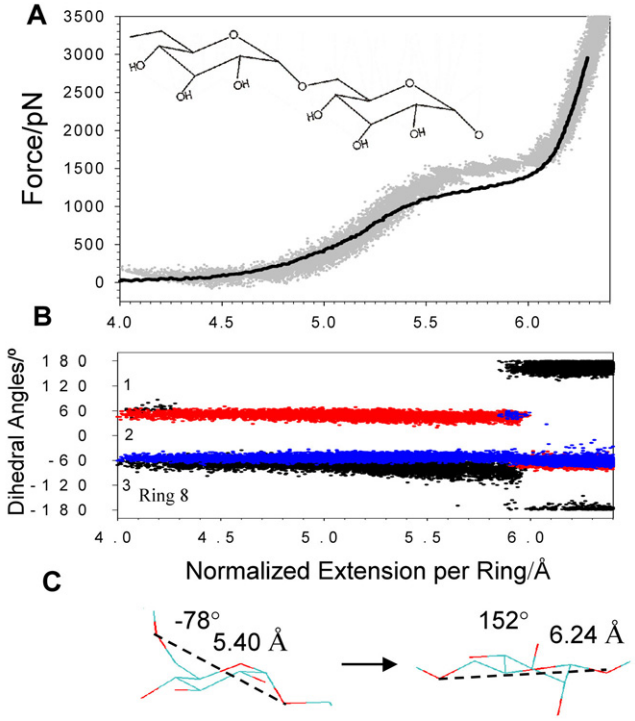

Figure 8. A 1 μs SMD simulation of dextran reproduces the AFM stretching curve. (A) A comparison between normalized force–extension curves of dextran obtained by SMD (grey trace) and by AFM (black trace). Inset: the structure of dextran showing two α-D-glucose rings connected by 1 $\rightarrow$ 6 linkage. (B) The conformational dynamics of ring No 8 during 1 μs simulation as revealed by the three torsions: $\omega = O_6$–C_6–C_5–O_5 (trace 3) indicates the rotameric status around the C_6–C_5 bond, and $t_1 = O_1$–C_1–C_2–O_2 (trace 1) and $t_2 = O_5$–C_5–C_4–C_3 (trace 2) indicate the conformational status of the glucose ring. (C) Two structures of ring No 8, extracted from the SMD simulation, reveal transition from a chair to a twist-boat conformation.

shown in figure 6 (top trace), is somewhat similar to amylose elasticity, with a pronounced plateau in the force–extension curve, albeit a plateau that starts at a much higher force ~700–1000 pN in dextran (Rief *et al* 1997, Marszalek *et al* 1998). Similar to the pustulan case, forced rotations about the C_5–C_6 bonds are expected to contribute to dextran elasticity. However, the axial deposition of the C_1–O_1 bonds in dextran suggests that, unlike those of pustulan, its ring structures may be susceptible to forced transitions to a boat-like conformation. SMD simulations of the dextran stretching process are invaluable in providing atomic insights into the behaviour of the glucose rings.

8.4. SMD simulations of dextran: forced rotations and chair–boat transitions

Figure 8(A) (grey trace) shows the results of a 1 μs SMD simulation of dextran in an implicit solvent (Lee *et al* 2004b). The SMD data closely follow the AFM measurements and this agreement allows us to propose a detailed model of the stretching process. An example of the behaviour of a dextran unit is shown in figure 8(B), which displays trajectories of the three torsions of the glucose ring during the SMD simulation. First, we note that, similarly to ring No 8 shown in figure 8(B), all the other rings end the stretching process in a boat-like, tg

conformation. This result indicates that dextran combines the elastic properties of pustulan ($1 \rightarrow 6$ linkages) and amylose (C_1–O_1 axial). Second, unlike pustulan, which experiences forced gt $\rightarrow$ tg transitions, dextran experiences gt $\rightarrow$ gg transitions, which occur at a very early stage of the stretching process. This is because the gg rotamer in dextran, but not in pustulan, provides an increased separation between atoms O_1 and O_6 in a conformation that is equi-energetic to that of the gt rotamer. Therefore, these low energy transitions do not contribute to the rising phase of the force–extension curve; they merely increase the contour length of dextran during the initial phase of the stretch. Third, once all the rings are in the gg state, stretching is dominated by a continuous bending of the ω torsion which is clearly captured by trace 3 in figure 8(B). This bending provides some chain extension and coincides with the rising phase of the force–extension profile that precedes the plateau feature. A careful analysis of the trajectories indicates that the onset of the plateau feature coincides with the onset of gg $\rightarrow$ tg rotations and ring instabilities. gg $\rightarrow$ tg rotations occur rapidly, as shown by a step-wise transition of trace 3 from $-80°$ to $-180°$, accompanied by a flip of the ring to a boat-like conformation, which is captured in trace 1 showing a flip of torsion t_1 from $+60°$ to $-60°$. The temporal analysis of the SMD trajectories, similar to that shown for ring No 8, suggests that rings in dextran undergo compound transformations: ${}^4C_{1,gg} \rightarrow T_{tg}$, where ${}^4C_{1,gg}$ represents the chair conformation with the C_6–O_6 bond in the gg state and T_{tg} represents a twist-boat with the C_6–O_6 bond in the tg orientation (figure 8(C)) (Lee *et al* 2004a, 2004b, Appell *et al* 2004). T_{tg} seems to work as a ratchet, which locks the ring conformation and secures the gain in the O_1–O_6 distance. Pure gg $\rightarrow$ tg rotations in the chair conformation also occur and they precede the final compound transition of the ring. However, they generate little gain in the O_1–O_6 distance, and this gain is not permanent because of the reverse transitions to the gg state. It is the transition to the final T_{tg} twist-boat structure, with the C_6–O_6 bond in the tg position and the C_1–O_1 bond in the quasi-equatorial orientation, that provides the maximum gain in the O_6–O_1 length which is permanent.

From this analysis we conclude that the extensibility of dextran is governed by a series of forced conformational transitions: the initial gt $\rightarrow$ gg transitions occur at very low forces and are followed by small changes in the orientation of the C_6–O_6 and C_1–O_1 bonds. These are followed by coupled chair–boat and gg $\rightarrow$ tg transitions to the final T_{tg} conformation of the ring (Lee *et al* 2004b).

9. How much work do atomic cranks and levers perform during stretching of pustulan and dextran?

From the normalized force–extension curves of pustulan, dextran and methylcellulose (figure 6), it is possible to estimate the work which is needed to rotate the C_6–O_6 crank and to flip the ring to a boat-like conformation. This work is in excess of the minimum work that is necessary to reduce the entropy of a simple freely jointed chain (e.g. methylcellulose) during stretching. This can be done by calculating, in each case, the increase in the free energy of the polysaccharide chain, ΔG, when stretched to a given extension l_{max}. ΔG can be calculated as the *reversible* work of the stretching force:

$$\Delta G = \int_0^{l_{max}} F \, dx.$$

This work can be measured by integrating the area under the force–extension curve. By calculating the areas under the normalized force curves in figure 6 up to a force of 1500 pN we find that $w_{cell} = 4.9$ kcal mol^{-1}/ring, $w_{pust} = 10.7$ kcal mol^{-1}/ring and $w_{dex} = 16.8$ kcal mol^{-1}/ring (Lee *et al* 2004b). The work to rotate the C_6–O_6 'crank' to

the tg orientation is, then, $w_{\rm rot} = w_{\rm pust} - w_{\rm cell} = 5.8$ kcal mol^{-1}/bond. Similarly, the work of the C_1–O_1 'lever' and the C_6–O_6 crank to flip the ring to the $T_{\rm tg}$ twist-boat conformation is $w_{c-b,{\rm tg}} = w_{\rm dex} - w_{\rm cell} = 11.9$ kcal mol^{-1}/ring (Lee *et al* 2004a, 2004b). Interestingly, the difference between $w_{c-b,{\rm tg}}$ and $w_{\rm rot}$ amounts to $\sim$6 kcal mol^{-1}, which is similar to the $\sim$5 kcal mol^{-1} necessary to flip the glucose ring to a boat-like conformation in amylose (Marszalek *et al* 1998).

10. Can force-induced conformational transitions play a role in biological systems?

It is possible that the conformational transitions that we reviewed here occur in biological systems, because polysaccharides and their sugar components are frequently placed under various mechanical stresses. Examples include polysaccharides in the cell wall of plants responding to changes in internal pressure. During adhesive interaction involving sugars and proteins, forces amounting to several hundred piconewtons per single bond between cells may occur (Puri *et al* 1998). Another example is provided by the lysozyme reaction in the cell walls of bacteria, where the enzyme forces the sugar ring into a highly strained conformation, before it severs the glycosidic linkage. Yet another example is provided by the enzymatic epimerization in seaweed alginates of β-D-mannuronic acid to α-L-guluronic acid by C-5 epimerase, with concomitant inversion of the pyranose ring from its $^4C_1$ to the $^1C_4$ chair structure and reorientation of the hydroxyls at C1 and C4 from the equatorial to the axial position. A similar reaction occurs in an important animal polysaccharide, heparin, where C-5 epimerase converts β-D-glucuronic acid (GlcA) to α-L-iduronic acid (IdoA), whose structure probably assumes a boat-like conformation in a functional complex between heparin and a protein antithrombin (Hricovini *et al* 2001, Hagner-McWhirter *et al* 2000). When β-1 $\rightarrow$ 6-linked sugars are subjected to tensile forces, the forced rotation of the C_6–O_6 bond to the tg orientation is expected to occur with a significant reorientation of the oxygen atom, O_6, to a new position where it could engage in a hydrogen bonding to stabilize a biologically important interaction. In α-1 $\rightarrow$ 6-linked sugars placed under tension, a shift of the gt/gg equilibrium towards the tg position is expected, with a similar effect. It is possible that strong adhesive forces acting on α-1 $\rightarrow$ 4- and α-1 $\rightarrow$ 6-linked sugars could flip the sugar ring to a boat-like structure (amylose, dextran) or an inverted chair conformation (pectin). Such a transition would result in a significant reorientation of the side groups allowing them to engage in or disengage from hydrogen bonding interactions with a protein (Drickamer 1997) to modulate, in a force-dependent manner, some biological activity of the latter.

11. Conclusions

We reviewed the elastic properties of individual polysaccharides derived from AFM and SMD experiments. We point to a significant role of axial glycosidic linkages in affecting the elasticity of α-linked polysaccharides. These bonds act as atomic levers that mechanically control the structure of the sugar rings and under tension can flip the ring to various high energy conformations such as a boat (twist) or an inverted chair. We discussed the role of atomic cranks and levers in forced rotations and complex chair–boat transitions coupled to rotations in 1 $\rightarrow$ 6-linked polysaccharides. We provide an estimate for the work that needs to be done by external forces to rotate atomic cranks and to flip atomic levers during the stretching of polysaccharide chains. By exploiting SMD simulations we are able to correctly interpret the results of single-molecule AFM measurements and gain insight into the conformational mechanics of sugar rings. It is possible that the conformational transitions that are induced in

sugar rings by AFM manipulations mimic the rearrangements that occur in polysaccharides in biological settings.

Acknowledgments

This work was supported by a grant from the National Science Foundation (MCB-0243360) and by Duke University funds to PEM.

References

Appell M, Strati G, Willett J L and Momany F A 2004 B3LYP/6-311+ + G** study of α- and β-D-glucopyranose and 1, 5-anhydro-D-glucitol: $^{4}C_{1}$ and $^{1}C_{4}$ chairs, $^{3,O}B$ and $B_{3,O}$ boats, and skew-boat conformations *Carbohydr. Res.* **339** 537–51

Barrows S E, Dulles F J, Cramer Ch J, French A D and Truhlar D G 1995 Relative stability of alternative chair forms and hydroxymethyl conformations of β-D-glucopyranose *Carbohydr. Res.* **276** 219–51

Barton D H R 1970 The principles of conformational analysis *Science* **169** 539–44

Brant D A 1999 Novel approaches to the analysis of polysaccharide structures *Curr. Opin. Struct. Biol.* **9** 556–62

Brunger A 1992 *X-PLOR, Version 3.1: A system for X-ray Crystallography and NMR* Yale University

Bustamante C, Bryant Z and Smith S B 2003 Ten years of tension: single-molecule DNA mechanics *Nature* **421** 423–7

Bustamante C, Marko J F, Siggia E A and Smith S 1994 Entropic elasticity of α-phage DNA *Science* **265** 599–600

Bustamante C, Smith S B, Liphardt J and Smith D 2000 Single-molecule studies of DNA mechanics *Curr. Opin. Struct. Biol.* **10** 279–85

Drickamer K 1997 Making a fitting choice: common aspects of sugar-binding sites in plant and animal lectins *Structure* **5** 465–8

Fisher T E, Marszalek P E and Fernandez J M 2000 Stretching single molecules into novel conformations using the atomic force microscope *Nat. Struct. Biol.* **7** 719–24

Florin E L, Rief M, Lehmann H, Ludwig M, Dornmair C, Moy V T and Gaub H E 1995 Sensing specific molecular interactions with the atomic force microscope *Biosens. Bioelectron.* **10** 895–901

Flory P J 1953 *Principles of Polymer Chemistry* (Ithaca, NY: Cornell University Press)

French A D, Rowland R S and Allinger N L 1990 Modeling of glucopyranose. The flexible monomer of amylose *Computer Modeling of Carbohydrate Molecules* (*ACS Symposium Series*) ed A D French and J W Brady (Washington, DC: American Chemical Society) pp 121–40

Gao M, Lu H and Schulten K 2002 Unfolding of titin domains studied by molecular dynamics simulations *J. Muscle Res. Cell Motil.* **23** 513–21

Grubmüller H, Heymann B and Tavan P 1996 Ligand binding and molecular mechanics calculation of the streptavidin–biotin rupture force *Science* **271** 997–9

Hagner-McWhirter A, Lindhal U and Li J-P 2000 Biosynthesis of heparin/heparan sulphate: mechanism of epimerization of glucuronyl C-5 *Biochem. J.* **347** 69–75

Hellerqvist C G, Lindberg B and Samuelsson K 1968 Methylation analysis of pustulan *Acta Chem. Scand.* **22** 2736

Hricovini M, Guerrini M, Bisio A, Torri G, Petitou M and Casu B 2001 Conformation of heparin pentasaccharide bound to antithrombin III *Biochem. J.* **359** 265–72

Isralewitz B, Gao M and Schulten K 2001 Steered molecular dynamics and mechanical functions of proteins *Curr. Opin. Struct. Biol.* **11** 224–30

Izrailev S, Stepaniants S, Balsera M, Oono Y and Schulten K 1997 Molecular dynamics study of unbinding of the avidin–biotin complex *Biophys. J.* **72** 1568–81

Jarvis M 2003 Chemistry–cellulose stacks up *Nature* **426** 611–2

Kalé L, Skeel R, Bhandarkar M, Brunner R, Gursoy A, Krawetz N, Phillips J, Shinozaki A, Varadarajan K and Schulten K 1999 NAMD2: greater scalability for parallel molecular dynamics *J. Comput. Phys.* **151** 283–312

Kirschner K N and Woods R J 2001 Solvent interaction determine carbohydrate conformation *Proc. Natl Acad. Sci. USA* **98** 10541–5

Kuttel M, Brady J W and Naidoo K J 2002 Carbohydrate solution simulations: producing a force field with experimentally consistent primary alcohol rotational frequencies and populations *J. Comput. Chem.* **23** 1236–43

Lee G, Nowak W, Jaroniec J, Zhang Q and Marszalek P E 2004a Nanomechanical control of glucopyranose rotamers *J. Am. Chem. Soc.* **126** 6218–9

Lee G, Nowak W, Jaroniec J, Zhang Q and Marszalek P E 2004b Molecular dynamics simulations of forced conformational transitions in 1,6-linked polysaccharides *Biophys. J.* **87** 1456–65

Li H, Rief M, Oesterhelt F and Gaub H E 1998 Single-molecular force spectroscopy on Xanthan by AFM *Adv. Mater.* **10** 316–9

Li H, Rief M, Oesterhelt F, Gaub H E, Zhang X and Shen J 1999 Single-molecule force spectroscopy on polysaccharides by AFM—nanomechanical fingerprint of α-(1, 4)-linked polysaccharides *Chem. Phys. Lett.* **305** 197–201

Lindberg B and McPherson J 1954 Studies on the chemistry of lichens. VI. The structure of Pustulan *Acta Chem. Scand.* **8** 985–8

Lu Z, Nowak W, Lee G, Marszalek P E and Yang W 2004 The elastic properties of single amylose chains in water: a quantum mechanical and AFM study *J. Am. Chem. Soc.* **126** 9033–41

Marszalek P E, Li H and Fernandez J M 2001 Fingerprinting polysaccharides with single molecule AFM *Nat. Biotechnol.* **19** 258–62

Marszalek P E, Li H, Oberhauser A F and Fernandez J M 2002 Chair–boat transitions in single polysaccharide molecules observed with force-ramp AFM *Proc. Natl Acad. Sci. USA* **99** 4278–83

Marszalek P E, Lu H, Li H, Carrion-Vazquez M, Oberhauser A F, Schulten K and Fernandez J M 1999b Mechanical unfolding intermediates in titin modules *Nature* **402** 100–3

Marszalek P E, Oberhauser A F, Li H and Fernandez J M 2003 The force driven conformations of heparin studied with single molecule force microscopy *Biophys. J.* **85** 2696–704

Marszalek P E, Oberhauser A F, Pang Y-P and Fernandez J M 1998 Polysaccharide elasticity governed by chair–boat transitions of the glucopyranose ring *Nature* **396** 661–4

Marszalek P E, Pang Y-P, Li H, Yazal J E, Oberhauser A F and Fernandez J M 1999a Atomic levers control pyranose ring conformations *Proc. Natl Acad. Sci. USA* **96** 7894–8

Momany F A and Willett J L 2000 Computational studies on carbohydrates: solvation studies on maltose and cyclomaltooligosaccharides (cyclodextrins) using a DFT/*ab initio*-derived empirical force field, AMB99C *Carbohydr. Res.* **326** 210–26

Nishiyama Y, Sugiyama J, Chanzy H and Langan P 2003 Crystal structure and hydrogen bonding system in cellulose 1(alpha), from synchrotron X-ray and neutron fiber diffraction *J. Am. Chem. Soc.* **125** 14300–6

Oberhauser A F, Marszalek P E, Erickson H P and Fernandez J M 1998 The molecular elasticity of the extracellular matrix protein tenascin *Nature* **393** 181–5

O'Donoghue P and Luthey-Schulten Z A 2000 Barriers to forced transitions in polysaccharides *J. Phys. Chem.* B **104** 10398–405

Pensak D A and French A D 1980 Conformational differences and steric energies for compounds containing α-D-glucopyranose chairs having a range of O-4-O-1 distances *Carbohydr. Res.* **87** 1–10

Pickett H M and Strauss H L 1970 Conformational structure, energy, and inversion rates of cyclohexane and some related oxanes *J. Am. Chem. Soc.* **92** 7281–90

Puri K D, Chen S and Springer T A 1998 Modifying the mechanical property and shear threshold of L-selectin adhesion independently of equilibrium properties *Nature* **392** 930–3

Rao V S R, Qasba P K, Balaji P V and Chandrasekaran R 1998 *Conformation of Carbohydrates* (Amsterdam: Harwood Academic)

Rief M, Fernandez J M and Gaub H E 1998 Elastically coupled two-level-systems as a model for biopolymer extensibility *Phys. Rev. Lett.* **81** 4764–7

Rief M, Oesterhelt F, Heymann B and Gaub H E 1997 Single molecule force spectroscopy on polysaccharides by atomic force microscopy *Science* **275** 1295–7

Tvaroška I, Taravel F R, Utille J P and Carver J P 2002 Quantum mechanical and NMR spectroscopy studies on the conformations of the hydroxymethyl groups in aldohexosides *Carbohydr. Res.* **337** 353–67

Weimar T, Kreis U C, Andrews J S and Pinto B M 1999 Conformational analysis of maltoside heteroanologues using high-quality NOE data and molecular mechanics calculations. Flexibility as a function of the interglycosidic chacogen atom *Carbohydr. Res.* **315** 222–33

Whistler R L and BeMiller J N 1993 *Industrial Gums. Polysaccharides and Their Derivatives* (San Diego, CA: Academic)